

arXiv:0909.1636v3 [astro-ph.HE] 18 Apr 2017

Relativistic Rayleigh-Taylor Instability of a Decelerating Shell and its Implications for Gamma Ray Bursts

Amir Levinson*

Raymond and Beverly Sackler School of Physics & Astronomy, Tel Aviv University, Tel Aviv 69978, Israel

(v3.3 released February 2009)

Global linear stability analysis of a self-similar solution describing the interaction of a relativistic shell with an ambient medium is performed. The solution is shown to be unstable to convective Rayleigh-Taylor modes having angular scales smaller than the causality scale. Longer wavelength modes are stable and decay with time. For modes of sufficiently large spherical harmonic degree l the dimensionless growth rate scales as $\sqrt{l/\Gamma}$, where Γ is the Lorentz factor of the shell. The instability commences at the contact interface separating the shocked ejecta and shocked ambient gas and propagates to the shocks. The reverse shock front responds promptly to the instability and exhibits rapidly growing distortions at early times. Propagation to the forward shock is slower, and it is anticipated that the region near the contact will become fully turbulent before the instability is communicated to the forward shock. The non-universality of the Blandford-McKee blast wave solution suggests that turbulence generated by the instability in the shocked ambient medium may decay slowly with time and may be the origin of magnetic fields over a long portion of the blast wave evolution. It is also speculated that the instability may affect the emission from the shocked ejecta in the early post-prompt phase of GRBs.

Keywords: Relativistic hydrodynamics; Shock waves; Instabilities; Gamma-ray bursts

1 Introduction

Relativistic shock waves is a common phenomenon in astrophysics. They form when a relativistic flow ejected by a compact central engine interacts with the surrounding medium or, in case of an intermittent source, as a result of steepening of waves produced in the outflow itself. The broadband emission observed in blazars, micro-quasars and gamma-ray bursts (GRBs) is produced behind those shocks and is an important diagnostic of the dissipation process.

Despite an impressive progress in our understanding of relativistic shocks some outstanding problems remain open. Of particular interest is the relativistic blast wave that form in GRB explosions when the relativistic ejecta expelled by the source impact the circumburst medium. The afterglow emission observed in most long GRBs is most likely produced in the thin layer enclosed between the forward shock and the ejecta, and is an important diagnostic of the blast wave evolution and the conditions in the shocked layer. Although the simple blast wave model has been quite successful in explaining the late afterglow evolution, recent observational efforts revealed some features that require extension of the simple model: (i) Observations of the late afterglow emission indicate strong amplification of magnetic fields in the post shock region - by several orders of magnitudes larger than what can be achieved by compression of the ambient magnetic field. Despite recent efforts to investigate potential mechanisms by which magnetic fields can be generated or amplified in the vicinity of the shock, this issue remains unresolved. (ii) SWIFT observations during the early afterglow phase reveal strong deviation of the lightcurve at early times from that predicted by the simple blast wave model. Several *ad hoc* explanations have been offered, including prolonged activity of the central engine and evolution of microphysical parameters. However, the feasibility of these scenarios depends on poorly understood physics, and it remains to be demonstrated that they can be derived from first principles. (iii) In the fireball scenario commonly adopted, the naive

*Corresponding author. Email: Levinson@wise.tau.ac.il

expectation has been that the crossing of the reverse shock should produce an observable optical flash. Despite considerable observational efforts, such flashes seem to be very rare. One plausible explanation is that the ejecta is magnetically dominated (Levinson and Eichler 1993, Lyutikov and Blandford 2003, Giannios and Spruit 2005, Giannios *et al.* 2008). Poynting flux dominated outflows have the advantage that they can naturally account for the ultra-relativistic Lorentz factors inferred. On the other hand, they are challenged by the rapid dissipation of magnetic energy that seems to be required. Furthermore, even if the flow is magnetically dominated some accumulation of baryon rich matter at the 'piston's' head is anticipated during the shock breakout phase, that may mimic effects of a hydrodynamic ejecta.

In this paper we explore the stability of the double-shock system. Hydrodynamic instabilities can give rise to strong distortions of the structure that may generate turbulence, amplify magnetic fields, and affect the emission processes in the post-prompt phase. Such effects have been studied in the non-relativistic case in connection with young supernovae remnants (SNRs). In fact, the idea that the Rayleigh-Taylor (R-T) instability should play an important role in the deceleration of a non-relativistic ejecta dates back to Gull (1973), who performed 1D simulations of young SNRs that incorporate a simple model of convection. Chevalier *et al.* (1992) later performed a global linear stability analysis of a self-similar solution describing the interaction of non-relativistic ejecta with an ambient medium and found that it is subject to a convective instability. They analyzed self-similar perturbations and showed that the flow is unstable for modes having angular scales smaller than some critical value. The convective growth rate was found to be largest at the contact discontinuity surface and to increase with increasing l number of the eigenmodes. They also performed 2D hydrodynamical simulations that verified the linear results and enabled them to study the nonlinear evolution of the instability. The simulation exhibits rapid growth of fingers from the contact interface that saturates, in the nonlinear state, by the Kelvin-Helmholtz instability. Strong distortions of the contact and the reverse shock was observed with little effect on the forward shock. Jun and Norman (1996) performed 2 and 3D MHD simulations of the instability to study the evolution of magnetic fields in the convection zone. They confirmed the rapid growth of small scale structure reported in (Chevalier *et al.* 1992), and in addition found strong amplification of ambient magnetic fields in the turbulent flow around R-T fingers. On average, the magnetic field energy density reaches about 0.5% of the energy density of the turbulence, but it could well be that the magnetic field amplification was limited by numerical resolution in their simulations. The simulations of Chevalier *et al.* (1992) and Jun and Norman (1996) support earlier ideas, that the clumpy shell structure observed in young (pre-Sedov stage) SNRs such as Tycho, Kepler and Cas A is due to the R-T and K-H instability.

In this paper we extend the linear stability analysis of Chevalier *et al.* (1992) into the relativistic regime. A preliminary account of the model and results is presented in (Levinson 2009). We find that denser ejecta sweeping a lighter ambient gas are subject to the R-T instability also in the relativistic case. The reason is that in the rest frame of the decelerating contact there is an effective gravitational force which is directed outwards, and so in this frame the denser ejecta is 'on top' of the lighter ambient gas. The stability of a double-shock system has been investigated by Wang *et al.* (2002) using the thin shell approximation. However, this study is limited to large scale modes and neglects pressure gradients and, therefore, precludes the convective instability. Thompson (2006) pointed out that a magnetized photon-rich shell that propagates through a dense Wolf-Rayet wind may be subject to the R-T instability. Using heuristic arguments he examined the conditions under which the instability develops and estimated the growth rate. The scaling of the growth rate found below is consistent with his result. Gruzinov (2000) performed a linear stability analysis of a Blandford-McKee (BMK) blast wave solution (Blandford and McKee 1976), and found that the BMK solution is stable but non-universal, in the sense that some modes decay very slowly as the system evolves. Furthermore, the onset of oscillations of an eigenmode of order l has been seen in the simulation once the Lorentz factor evolved to $\Gamma < l$. The conclusion drawn based on Gruzinov's findings is that distortion of the shock front at early times may cause significant oscillations during a large portion of its evolution. If the amplitude of these oscillations is sufficiently large, and if the same behavior holds in the nonlinear regime then this can lead to generation of vorticity in the post shock region (Goodman and MacFadyen 2008, Milosavljevic and Nakar 2007), and the consequent amplification of magnetic fields, as demonstrated recently by Zhang *et al.* (2009).

The plan of the paper is as follows: In section 2 we derive the basic equations in a general form. In

section 3 a class of self-similar solutions for the double-shock structure, obtained originally by Nakamura and Shigeyama (2006), is reviewed. These are employed as the unperturbed solutions for our analysis. The linear perturbation analysis of these solutions is presented in section 4. The implications for gamma-ray bursts are discussed in section 5. We conclude in section 6. Detailed derivation of main results is given in the appendices.

2 Basic equations

Consider an unmagnetized fluid, and let ρ , p , \tilde{h} and u^μ denote its proper density, pressure, dimensionless specific enthalpy, and 4-velocity, respectively. The stress-energy tensor then takes the form

$$T^{\mu\nu} = \rho\tilde{h}u^\mu u^\nu - g^{\mu\nu}p, \quad (1)$$

where $g^{\mu\nu}$ is the metric tensor. Neglecting radiative losses, the dynamics of the flow is governed by mass and energy-momentum conservation:

$$\partial_\mu(\rho u^\mu) = 0, \quad \partial_\mu T^{\mu\nu} = 0. \quad (2a,b)$$

Using (2a) the different components of (2b) reduce to

$$W \frac{d \ln \gamma}{dt} + \gamma^2 \frac{dp}{dt} = \frac{\partial p}{\partial t}, \quad (3a)$$

$$\frac{d}{dt} \ln(p/\rho^{\hat{\gamma}}) = 0, \quad (3b)$$

$$\rho\gamma \frac{d}{dt}(\tilde{h}\gamma\mathbf{v}_T) + \nabla_T p = 0. \quad (3c)$$

Here $\gamma = u^0$ is the Lorentz factor of the fluid, \mathbf{v}_T is the tangential component of the 3-velocity, which we express as $\mathbf{v} = v_r \hat{\mathbf{r}} + \mathbf{v}_T$, $\hat{\gamma}$ is the adiabatic index, $W = \rho\tilde{h}\gamma^2$, $d/dt = (u^\mu/u^0)\partial_\mu$ is the convective derivative, and

$$\nabla_T \equiv \hat{\theta} \frac{1}{r} \frac{\partial}{\partial \theta} + \hat{\phi} \frac{1}{r \sin \theta} \frac{\partial}{\partial \phi}. \quad (4)$$

If the flow passes through a discontinuous shock front, then the solutions of the flow equations in the upstream and downstream regions are to be matched at the shock surface, which is defined by the equation $\psi(x^\mu) \equiv r - R(t, \theta, \phi) = 0$. Integration of (2a,b) across the surface lead to the jump conditions

$$[\rho u^\mu] n_\mu = 0, \quad [T^{\mu\nu}] n_\nu = 0, \quad (5a,b)$$

where the square brackets denote the difference of the enclosed quantity across the shock front, and

$$n_\mu = \frac{\partial_\mu \psi}{\sqrt{\partial_\mu \psi \partial^\mu \psi}} \quad (6)$$

is a 4-vector normal to the shock front.

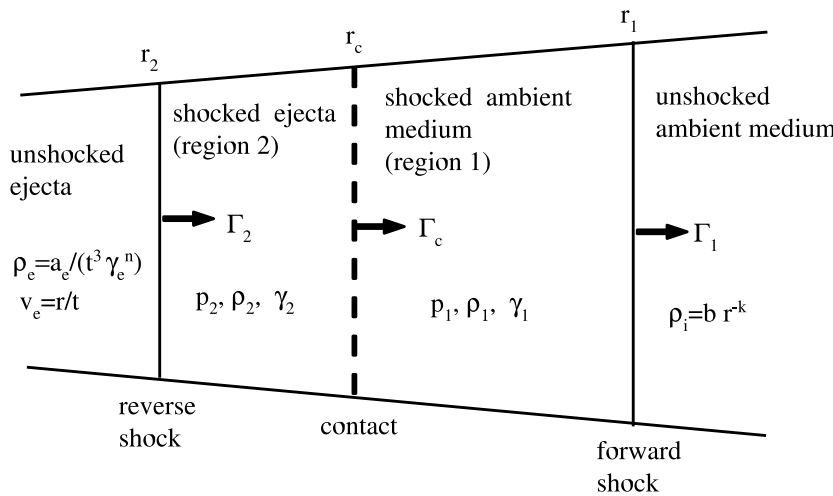


Figure 1. Schematic representation of the double-shock system. There are three characteristic surfaces: a forward shock propagating in the ambient medium, a reverse shock sweeping the ejecta, and a contact discontinuity separating the shocked ejecta and the shocked ambient medium. The Lorentz factors of the three surfaces, measured with respect to the unshocked ambient medium, are indicated. Quantities in the shocked ambient medium (region 1) and shocked ejecta (region 2) are denoted by subscripts 1 and 2, respectively.

3 Unperturbed solutions

The unperturbed solution invoked here is the self-similar solution derived by Nakamura and Shigeyama (2006). It is reviewed here to set up the notation and to introduce some aspects that are important for the stability analysis. Nakamura and Shigeyama considered a freely expanding ejecta interacting with an ambient medium having a density profile $\rho_i = br^{-k}$. The freely expanding ejecta is characterized by a velocity $v_e = r/t$ at time t after the explosion, and a proper density profile

$$\rho_e = \frac{a_e}{t^3 \gamma_e^n}, \quad (7)$$

where $\gamma_e = 1/\sqrt{1-v_e^2}$ is the corresponding Lorentz factor (it can be readily seen that the continuity equation (2a) is satisfied for this choice of ρ_e and v_e).

The system under consideration is shown schematically in figure 1. The subscript 1 refers to the shocked ambient medium and 2 to the shocked ejecta. The Lorentz factors of the forward shock, reverse shock and the contact discontinuity are denoted by $\Gamma_1(t)$, $\Gamma_2(t)$ and $\Gamma_c(t)$, respectively. Self-similarity requires that they all have a similar time evolution, viz., $\Gamma_2^2 = At^{-m}$, $\Gamma_1^2 = Bt^{-m}$, $\Gamma_c^2 = Ct^{-m}$, where A, B, C and m are constants determined upon matching the solutions in regions 1 and 2 at the contact discontinuity. The similarity parameter can be defined as (Blandford and McKee 1976)

$$\chi = [1 + 2(m+1)\Gamma_1^2](1-r/t). \quad (8)$$

The shocks and the contact are surfaces of constant χ , and since the velocity of a constant χ surface is

given by

$$\frac{dr}{dt} = 1 - \frac{\chi}{2\Gamma_1^2}, \quad (9)$$

we readily obtain $\chi_1 = 1$, $\chi_c = (\Gamma_1/\Gamma_c)^2 = B/C > 1$ and $\chi_2 = (\Gamma_1/\Gamma_2)^2 = B/A > \chi_c$. The trajectory of the reverse shock is

$$r_2(t) = \int_0^t \left(1 - \frac{1}{2\Gamma_2^2}\right) dt' = t - \frac{t}{2(m+1)\Gamma_2^2}, \quad (10)$$

from which we obtain for the velocity of the ejecta crossing the shock: $v_e(r_2) = r_2/t = 1 - 1/[2(m+1)\Gamma_2^2]$. The corresponding Lorentz factor is thus given, to order $O(\Gamma_2^{-2})$, by

$$\gamma_e^2 = (m+1)\Gamma_2^2, \quad (11a)$$

and the density by

$$\rho_e = \frac{a_e}{t^3\gamma_e^n} = \frac{a_e}{A^{3/m}(m+1)^{n/2}\Gamma_2^{(6/m)-n}}. \quad (11b)$$

3.1 Shocked ambient medium

We consider cases where the forward shock is ultra-relativistic. The specific enthalpy of the shocked ambient gas (region 1) is then approximated by $\tilde{h}_1 = 4p_1/\rho_1$. The jump conditions at the forward shock follow from (5a,b) and (6) using $R(t, \theta, \phi) = r_1(t) = t[1 - 1/2(m+1)\Gamma_1^2]$. The self-similar variables for the Lorentz factor, pressure and density are defined as

$$\gamma_1^2 = \frac{1}{2}\Gamma_1^2 g(\chi), \quad (12a)$$

$$\rho_1' = \rho_1\gamma_1 = 2\rho_i\Gamma_1^2 h(\chi), \quad (12b)$$

$$p_1 = \frac{2}{3}\rho_i\Gamma_1^2 f(\chi). \quad (12c)$$

Under this choice the shock jump conditions imply $g(1) = f(1) = h(1) = 1$. The equations obeyed by the variables g , f , h are outlined in Appendix A.1. Using (12a) the Lorentz factor of the contact surface can be written as $\Gamma_c = \Gamma_1\sqrt{g_c/2}$, where $g_c \equiv g(\chi_c)$, which combined with the relation $\chi_c = (\Gamma_1/\Gamma_c)^2$ derived above yields $\chi_c g_c = 2$. The solution is obtained by numerically integrating equations (A.2a-c) from the forward shock front $\chi = 1$ to the contact discontinuity where $g_c\chi_c = 2$. The quantities g_c , χ_c are eigenvalues of the solution.

3.2 Shocked ejecta

The reverse shock cannot be considered ultra-relativistic in general and, therefore, a complete treatment is required. The specific enthalpy of the shocked ejecta is taken to be $\tilde{h}_2 = 1 + \hat{\gamma}p_2/[\rho_2(\hat{\gamma} - 1)]$, and we remind that $\hat{\gamma}$ denotes the adiabatic index. Assuming the unshocked ejecta to be cold, the jump conditions at the reverse shock, obtained from (5a,b) and (6) using $R(t, \theta, \phi) = r_2(t)$, read

$$\rho_e\gamma_e(v_e - V_2) = \rho_2\gamma_2(v_2 - V_2), \quad (13a)$$

$$\rho_e\gamma_e^2(v_e - V_2) = W_2(v_2 - V_2) + P_2V_2, \quad (13b)$$

$$\rho_e\gamma_e^2v_e(v_e - V_2) = W_2v_2(v_2 - V_2) + P_2, \quad (13c)$$

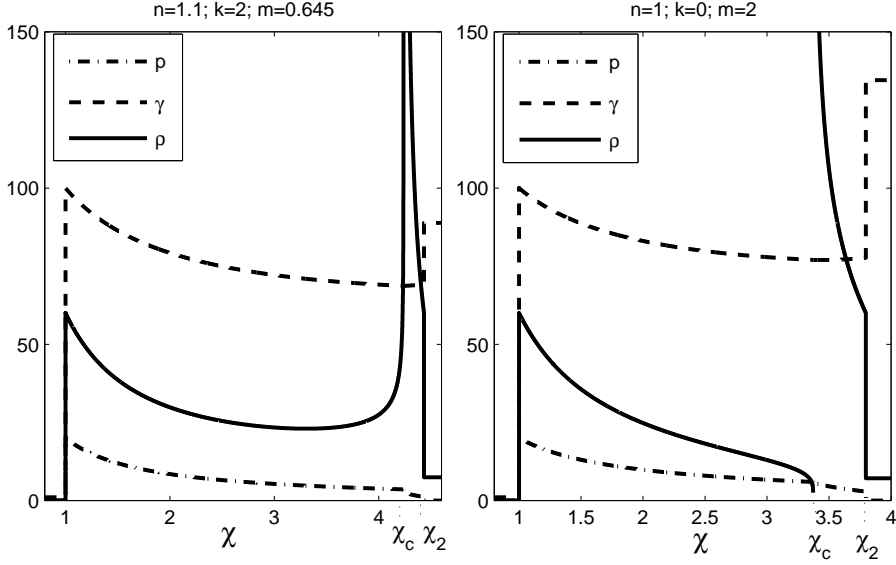


Figure 2. Profiles of the pressure, proper density and Lorentz factor of the unperturbed flow, for two different choices of parameters. The forward shock is located at $\chi = 1$. The location of the reverse shock (χ_2) and the contact discontinuity (χ_c) are indicated.

here $V_2 = dr_2/dt$ is the shock 3-velocity. Equations (13a-c) can be solved by employing (11a) and recalling that $W_2 = \rho_2 h_2 \gamma_2^2$. One finds

$$\gamma_2^2(\chi_2) = q\Gamma_2^2, \quad (14a)$$

$$\rho_2'(\chi_2) = \frac{mq\rho_e\gamma_e}{(m+1)(q-1)}, \quad (14b)$$

$$p_2(\chi_2) = \frac{m\rho_e}{a(q-1)+2} \left(1 - \sqrt{q/(m+1)}\right), \quad (14c)$$

where \sqrt{q} is the only positive solution of the equation

$$\hat{\gamma}x^3 + (2 - \hat{\gamma})\sqrt{m+1}x^2 - (2 - \hat{\gamma})x - \hat{\gamma}\sqrt{m+1}x = 0. \quad (15)$$

Following Nakamura and Shigeyama (2006) we find it convenient to transform in region 2 to a new similarity parameter,

$$\sigma = \chi/\chi_2 = \{1 + 2(m+1)\Gamma_2^2\}(1 - r/t). \quad (16)$$

The reverse shock is then located at $\sigma = 1$ and the contact at

$$\sigma_c = \chi_c/\chi_2 = \Gamma_2^2/\Gamma_c^2. \quad (17)$$

The self similar variables of the shocked ejecta, G , F , H , are then defined as

$$\gamma_2^2 = q\Gamma_2^2 G(\sigma), \quad (18a)$$

$$\rho_2' = \frac{mq\rho_e\gamma_e}{(m+1)(q-1)} H(\sigma), \quad (18b)$$

$$p_2 = \frac{m\rho_e}{a(q-1)+2} \left[1 - \sqrt{q/(m+1)}\right] F(\sigma), \quad (18c)$$

and satisfy $F(1) = G(1) = H(1) = 1$. From equations (17) and (18a) we obtain $G_c\sigma_c = 1/q$ at the

contact discontinuity. The equations obeyed by these self-similar variables are derived in Appendix A.2. The solution in this region is obtained upon integration of (A.4a-c) from the reverse shock $\sigma = 1$ to the contact $G_c\sigma_c = 1/q$.

3.3 Conditions at the contact surface

Two conditions at the contact discontinuity fix the constants A , B , and m . One condition is that there be no flow across the contact interface. This implies $\Gamma_c = \gamma_{1c} = \gamma_{2c}$, from which we obtain

$$\frac{\Gamma_1^2}{\Gamma_2^2} = \frac{B}{A} = 2q \frac{G_c}{g_c}, \quad (19)$$

where equations (12a) and (18a) have been employed. The second condition is pressure balance, viz., $p_1(t, \chi_c) = p_2(t, \sigma_c)$. This condition yields two relations. The first one,

$$m = \frac{6 - 2k}{n + 2}, \quad (20)$$

comes from the requirement that p_1 and p_2 have the same time dependence. The second one is implied by equations (12c) and (18c):

$$\frac{a_e}{bA^{1+n/2}} = \frac{4q[\hat{\gamma}(q-1) + 2(\hat{\gamma}-1)]}{3m(\hat{\gamma}-1)} \frac{G_c f_c}{g_c F_c} \left(\frac{m+1}{\sigma_c} \right)^{n/2} \left(1 - \sqrt{\frac{q}{m+1}} \right)^{-1}. \quad (21)$$

The solution described above is valid for $-1 < m < 3 - k$ (Blandford and McKee 1976). The case $m = 3 - k$ corresponds to an adiabatic impulsive blast wave (for which $g_\chi = 1$ so that the contact surface is undefined). From (A.2a-c) it can be shown (Blandford and McKee 1976) that near the contact discontinuity the density of the ambient medium behaves as $h \propto (2 - g_\chi)^{-\theta_1}$, with $\theta_1 = (m - k)/(m + 3k - 12)$. Thus, within the range of parameters for which the solution is valid h diverges at the contact for $m < k$ and vanishes for $m > k$. Likewise, from (A.4a-c) we find that the density of the shocked ejecta behaves as $H \propto (qG\sigma - 1)^{-\theta_2}$, where $\theta_2 = (1 - \hat{\gamma})(mn - 6)/(10\hat{\gamma} + 2mn - 12) = (\hat{\gamma} - 1)(6 + nk)/[5\hat{\gamma}(n + 2) - 2nk - 12]$. Within the allowed range of parameters θ_2 is always positive, so that H always diverges. This is seen in figure 2, where solutions obtained for an ejecta interacting with a uniform density medium (right panel) and a stellar wind (left panel) are exhibited.

4 Global linear stability analysis

We now consider linear perturbations of the self-similar solution described above. As shown below, unlike in the non-relativistic case (Chevalier *et al.* 1992) the relativistic perturbation equations do not admit self-similar solutions, with the exception of the spherical mode. The reason is the inherent coupling, via the Lorentz factor, of the radial and tangential velocity perturbations δv_r and δv_T . Thus, numerical integration of the time dependent equations is required.

4.1 Perturbation equations

The perturbed variables are taken to be

$$\rho' = \rho'_0(t, r) + \delta\rho'(t, r, \theta, \phi), \quad (22a)$$

$$p = p_0(t, r) + \delta p(t, r, \theta, \phi), \quad (22b)$$

$$\mathbf{v} = v_0(r)\hat{\mathbf{r}} + \delta v_r(r, \theta, \phi)\hat{\mathbf{r}} + \delta \mathbf{v}_T(r, \theta, \phi), \quad (22c)$$

here the subscript zero denotes the unperturbed flow. To simplify the notation we define $d_t^0 = \partial_t + v_0 \partial_r$ to be the convective derivative with respect to the unperturbed flow. The Lagrangian change of some quantity Q is then given to first order by $dQ/dt = d_t^0(Q_0 + \delta Q) + \delta v_r \partial_r Q_0$. The linearized equations for the perturbations, obtained upon substitution of the expressions (22a-c) into the hydrodynamic equations (3a-c) are

$$d_t^0(\delta\rho'/\rho'_0) + \partial_r \delta v_r + (2/r + \partial_r \ln \rho'_0) \delta v_r + \nabla(\delta \mathbf{v}_T) = 0, \quad (23a)$$

$$d_t^0 \left(\frac{\delta p}{p_0} - \hat{\gamma} \frac{\delta \rho'}{\rho'_0} + \hat{\gamma} \frac{\delta \gamma}{\gamma_0} \right) + \delta v_r \partial_r \ln(p_0 \rho_0^{-\hat{\gamma}}) = 0, \quad (23b)$$

$$\rho'_0 d_t^0(\tilde{h}_0 \gamma_0 \delta \mathbf{v}_T) + \nabla_T \delta p = 0, \quad (23c)$$

$$W_0 [d_t^0(\gamma_0^2 \delta v_r) + \delta v_r \partial_r \ln \gamma_0] + \delta W d_t^0(\ln \gamma_0) + \gamma_0^2 d_t^0 \delta p + \gamma_0^2 \delta v_r [2\gamma_0^2 d_t^0 p_0 + \partial_r p_0] - \partial_t \delta p = 0. \quad (23d)$$

Next, we apply the perturbation equations (23a-d) to regions 1 and 2 (see figure 1), using the self-similar solutions in each region for the unperturbed quantities.

4.1.1 Perturbed flow in region 1. We expand the perturbations in spherical harmonics and use χ and $\tau = \ln t$ as new independent variables in place of r, t . The perturbations in region 1 are then expressed as

$$\delta\rho'_1 = \rho'_{10} \xi_\rho(\tau, \chi) Y_{l\tilde{m}}(\theta, \phi), \quad (24a)$$

$$\delta p_1 = p_{10} \xi_P(\tau, \chi) Y_{l\tilde{m}}(\theta, \phi), \quad (24b)$$

$$\delta v_{1r} = \frac{1}{\Gamma_1^2 g} \xi_R(\tau, \chi) Y_{l\tilde{m}}(\theta, \phi), \quad (24c)$$

$$\delta \mathbf{v}_{1T} = \xi_T(\tau, \chi) r \nabla_T Y_{l\tilde{m}}(\theta, \phi), \quad (24d)$$

with ρ'_{10} and p_{10} given by (12b,c), respectively. When these expressions are substituted in equations (23a-d) a set of first order hyperbolic PDEs for the dimensionless amplitudes ξ_α is obtained:

$$\partial_\tau \xi_\alpha = \Sigma_\beta \{ A_{\alpha\beta} \partial_\chi \xi_\beta + B_{\alpha\beta} \xi_\beta \}, \quad (25)$$

where the indices α, β run over R, P, ρ, T . The details are given in Appendix B.1. The coefficients $A_{\alpha\beta}$ and $B_{\alpha\beta}$, given explicitly in (B.4a-c) and (B.5a-g), are functions of the self-similarity coordinate χ , but are independent of τ .

4.1.2 Perturbed flow in region 2. Likewise, in region 2 we transform to the coordinates σ, τ and define

$$\delta\rho'_2 = \rho'_{20} \eta_\rho(\tau, \sigma) Y_{l\tilde{m}}(\theta, \phi), \quad (26a)$$

$$\delta p_2 = p_{20} \eta_P(\tau, \sigma) Y_{l\tilde{m}}(\theta, \phi), \quad (26b)$$

$$\delta v_{2r} = \frac{1}{\Gamma_2^2 G} \eta_R(\tau, \sigma) Y_{l\tilde{m}}(\theta, \phi), \quad (26c)$$

$$\delta \mathbf{v}_{2T} = \eta_T(\tau, \sigma) r \nabla_T Y_{l\tilde{m}}(\theta, \phi). \quad (26d)$$

The unperturbed parameters of the shocked ejecta, ρ'_{20}, p_{20} are given by equations (18b,c). The derivation of the perturbation equations for the dimensionless perturbations η_α is presented in Appendix B.2. The resultant set of equations is

$$\partial_\tau \eta_\alpha = \Sigma_\beta \{C_{\alpha\beta} \partial_\chi \eta_\beta + D_{\alpha\beta} \eta_\beta\}, \quad (27)$$

with the coefficients $C_{\alpha\beta}(\sigma)$ and $D_{\alpha\beta}(\sigma)$ given explicitly in (B.8a-d) and (B.9a-h).

4.2 Boundary conditions

Equations (25), (27) are solved subject to boundary conditions imposed at the shock fronts and at the contact discontinuity. We allow perturbations of the shock fronts and the contact surface of the form

$$\delta r_a(t, \theta, \phi) = \frac{t \delta_a(t)}{\Gamma_a^2} Y_{l\tilde{m}}(\theta, \phi), \quad (28)$$

here $a = 1, 2, c$ refers to the forward shock, reverse shock, and the contact discontinuity, respectively. The corresponding perturbation of the 3-velocity at these surfaces is

$$\delta V_a = \Gamma_a^{-2} [\partial_\tau \delta_a + (m+1) \delta_a] Y_{l\tilde{m}}(\theta, \phi). \quad (29)$$

Now, the Lagrange perturbation of some fluid quantity Q at the perturbed position of surface a is given by $\Delta_a Q = (\partial_r Q_0) \delta r_a + \delta Q$; e.g., $\Delta_a \rho' = (\partial_r \rho'_0) \delta r_a + \delta \rho'$, etc. Defining $v^\mu = u^\mu / u^0$ and denoting by $n_{j\mu} = n_{j\mu}^0 + \delta n_{j\mu}$ the perturbed normal of the forward ($j = 1$)/reverse ($j = 2$) shock, equation (5a) gives to first order

$$[(\rho'_0 + \Delta_j \rho')(v_0^\mu + \Delta_j v^\mu)(n_{j\mu}^0 + \delta n_{j\mu})] = 0, \quad (30a)$$

and (5b)

$$[(W_0 + \Delta_j W)(v_0^\nu + \Delta_j v^\nu)(v_0^\mu + \Delta_j v^\mu) - (p_0 + \Delta_j p) g^{\nu\mu}] (n_{j\mu}^0 + \delta n_{j\mu}) = 0. \quad (30b)$$

The forward shock is described by the equation $\psi_1(x^\mu) = r - r_1(t) - \delta r_1(t, \theta, \phi)$, from which we obtain, using (6),

$$n_{1\mu}^0 = (-\Gamma_1 V_1, \Gamma_1, 0), \quad (31a)$$

$$\delta n_{1\mu} = (-\Gamma_1^3 \delta V_1, \Gamma_1^3 V_1 \delta V_1, -\Gamma_1 \nabla_T \delta r_1). \quad (31b)$$

The density, pressure, and Lorentz factor of the unshocked flow just upstream of the forward shock are $p_i = 0$, $\rho_i = b r^{-k}$, and $\gamma_i = 1$. At the perturbed shock front $\Delta_1 \rho_i = -k \rho_i \delta r_1 / r_1$ and can be neglected to the order to which we are working. Applying (24a-d) to the forward shock and using (30a), (31a,b) we get

$$\xi_\rho = \partial_\tau \delta_1 + 2\xi_R + (3m - 3 + 2k) \delta_1. \quad (32a)$$

Likewise, the transverse component of (30b) yields

$$\xi_T = -\delta_1 / \Gamma_1^2, \quad (32b)$$

and the other two components

$$\xi_P = 2\partial_\tau \delta_1 + (14 - 8m - 6k) \frac{\delta_1}{3}, \quad (32c)$$

$$\xi_R = 2\partial_\tau \delta_1 - 2(m - 3 + k) \delta_1. \quad (32d)$$

Finally, we eliminate δ_1 from equations (32c,d) to get three boundary conditions at the forward shock ($\chi = 1$):

$$\partial_\tau \xi_P - \partial_\tau \xi_R = (m - 3 + k)\xi_P + \frac{1}{3}(7 - 4m - 3k)\xi_R, \quad (33a)$$

$$\xi_T = \frac{3}{2(m+2)\Gamma_1^2}[\xi_P - \xi_R], \quad (33b)$$

$$\xi_\rho = -\partial_\tau(\Gamma_1^2 \xi_T) + 2\xi_R - (3m - 3 + 2k)\Gamma_1^2 \xi_T. \quad (33c)$$

As a check note that for the impulsive BMK solution with $m = 3$ and $k = 0$ equations (33a,b) reduce to those derived in (Gruzinov 2000).

The derivation of the boundary conditions at the reverse shock is far more involved. The details are presented in Appendix C. One finds

$$\partial_\tau \eta_R = -\frac{d_{sP} - f_{sP}d_{s\rho}}{d_{sR} - f_{sR}d_{s\rho}}\partial_\tau \eta_P - \frac{1 - f_{s\delta}d_{s\rho}}{d_{sR} - f_{sR}d_{s\rho}}\partial_\tau \delta_2, \quad (34a)$$

$$\partial_\tau \eta_\rho = -f_{sR}\partial_\tau \eta_R - f_{sP}\partial_\tau \eta_P - f_{s\delta}\partial_\tau \delta_2, \quad (34b)$$

$$\eta_T = -\frac{2}{\kappa(q-1)\Gamma_2^2}[d_{sR}\eta_R + d_{sP}\eta_P + d_{s\rho}\eta_\rho], \quad (34c)$$

$$\partial_\tau \delta_2 = -e_{sR}\eta_R - e_{sP}\eta_P - e_{s\rho}\eta_\rho, \quad (34d)$$

at $\sigma = 1$. The coefficients are given in (C.11a-c) of Appendix C.

Two additional boundary conditions are imposed at the contact discontinuity. The requirement that there be no flow across the contact surface, that is $v - dr_c/dt = 0$, implies $\partial_r v_0 \delta r_c + \delta v_r - d_t^0 \delta r_c = 0$ on each side of that surface. Upon substitution of the unperturbed solution we obtain

$$\partial_\tau \delta_c = \frac{\xi_R(\tau, \chi_c)}{2} - (m+1)[1 + \chi_c(\partial_\chi \ln g)_c] \delta_c, \quad (35a)$$

$$\partial_\tau \delta_c = q\eta_R(\tau, \sigma_c) - (m+1)[1 + \sigma_c(\partial_\sigma \ln G)_c] \delta_c, \quad (35b)$$

where subscript c refers to values at the contact. Pressure balance across the contact discontinuity yields

$$\eta_P(\tau, \sigma_c) - \xi_P(\tau, \chi_c) = 2(m+1)[\sigma_c(\partial_\sigma \ln F)_c - \chi_c(\partial_\chi \ln f)_c] \delta_c. \quad (35c)$$

After some manipulation of (35a-c) we finally arrive at

$$\begin{aligned} \partial_\tau \xi_R(\tau, \chi_c) - 2q\partial_\tau \eta_R(\tau, \sigma_c) &= -(m+1)[1 + \sigma_c(\partial_\sigma \ln G)_c]\xi_R(\tau, \chi_c) \\ &\quad + 2q(m+1)[1 + \chi_c(\partial_\chi \ln g)_c]\eta_R(\tau, \sigma_c), \end{aligned} \quad (36a)$$

$$\eta_P(\tau, \sigma_c) - \xi_P(\tau, \chi_c) = 2(m+1)\{\sigma_c \partial_\sigma \ln F)_c - \chi_c \partial_\chi \ln f)_c\} \delta_c, \quad (36b)$$

with

$$\delta_c(\tau) = \frac{\xi_R(\tau, \chi_c) - 2q\eta_R(\tau, \sigma_c)}{2(m+1)[\chi_c(\partial_\chi \ln g)_c - \sigma_c(\partial_\sigma \ln G)_c]}. \quad (36c)$$

Equations (33a-c), (34a-d) and (36a-c) provide a set of eight boundary conditions for the perturbation equations.

4.3 Numerical scheme

To integrate equations (25) and (27) we first transform to a new set of variables, the so called ‘‘Riemann invariants’’. In region 1 those are related to the old variables through

$$\xi_{\pm} = \frac{1}{\sqrt{3}}\xi_R \pm \frac{1}{2}\xi_P, \quad (37a)$$

$$\xi_3 = \xi_{\rho} - \xi_R/2 - 3\xi_P/4, \quad \xi_4 = \xi_T, \quad (37b,c)$$

and in region 2 through

$$\eta_{\pm} = \frac{\eta_R}{2} \pm \frac{1}{2q\sqrt{\kappa\hat{\gamma}}}\eta_P, \quad (38a)$$

$$\eta_3 = \eta_{\rho} - q\eta_R - \eta_P/\hat{\gamma}, \quad \eta_4 = \eta_T, \quad (38b,c)$$

with $\kappa(\sigma) = W_{20}/p_{20}\gamma_{20}^2$, as defined in Appendix A.2. The equations for the new variables can be obtained upon appropriate transformations of (25), (27), and are derived in Appendix D. As shown there, ξ_{-}, ξ_3, ξ_4 propagate from the forward shock to the contact discontinuity while ξ_{+} propagates in the opposite direction. Likewise, η_{+}, η_3, η_4 propagate from the reverse shock to the contact discontinuity whereas η_{-} propagates from the contact discontinuity to the reverse shock. Thus, the two boundary conditions at the contact discontinuity, (36a,b), are applied to ξ_{+} and η_{-} after appropriate transformation of variables, and the boundary conditions at the forward and reverse shocks to the remaining Riemann invariants.

Numerical simulations of equations (D.3) and (D.5) were performed using the forward Euler scheme with upwind differencing of spatial derivatives. We also used for comparison a 4th order Runge-Kutta routine with an adaptive step size to advance the equations in time and found unnoticeable differences between the two methods for all cases studied below. For each experiment we have made several runs with increasing grid resolution until the result converged. The divergence of the unperturbed density at the contact have caused no difficulties. To test the code we exploited the analytic solutions for the spherical modes obtained below. We generally found excellent agreement. As an example, for the choice $n = 1.1, k = 2$ for which $m = 0.645$, and with 10^4 grid points on each side of the contact discontinuity all of the Riemann invariants followed the analytic solution to an accuracy better than 10^{-4} up to a time $\tau = 5$ (or $t/t_0 = e^5$). The accuracy of the initial condition, specifically the accuracy at which the boundary conditions at the contact at $\tau = 0$ were matched was 4.8×10^{-5} in this run.

As a second test we solved (D.3) for an impulsive BMK solution with $k = 0$. For this solution a contact surface does not exist ($g\chi = 1$ for every χ), so the boundary condition for ξ_{+} at the contact needs to be replaced. We verified that the solution depends weakly on this condition provided it is fixed sufficiently far from the forward shock, at $\chi \gg 1$. We compared our result with that obtained in Gruzinov (2000) and found excellent agreement¹.

4.4 Spherical perturbations

For spherical perturbations ($l = 0$) the tangential velocity vanishes, viz., $\delta\mathbf{v}_T = 0$, as can be directly seen from (24d) and (26d). Then (25), (27) admit solutions of the form $\xi_{\alpha}(\chi, \tau) = \xi_{\alpha}(\chi)e^{s\tau}$, $\eta_{\alpha}(\sigma, \tau) = \eta_{\alpha}(\sigma)e^{s\tau}$; $\alpha = (R, P, \rho)$, where s is an eigenvalue determined from the boundary conditions at the contact discontinuity. There are two spherical modes. One is associated with a linear time translation of the unperturbed solution; that is, it is the difference between a solution at time t and a solution at time

¹There is a small error in Gruzinov (2000). The coefficient of the 3rd term on the right-hand side of his 30 should be $-17/3$ (see (B.3c)) and not $-14/3$ as in the astro-ph/0012364 version. However, we have confirmed that the effect of this error on the result is insignificant.

$t + \delta t$. Since to lowest order all surfaces propagate at the speed of light the distance between corresponding surfaces of the two solutions should remain δt at all times. This implies $\delta V_a = 0$ to order $O(\Gamma^{-2})$ and from (29) we anticipate that $s = -(m + 1)$ for this mode. From (8) and (16) it can be readily seen that the change in the self-similarity parameters χ and σ corresponding to a time translation δt is $\delta\chi = 2(m + 1)\Gamma_1^2 \delta t/t = 2(m + 1)B e^{-(m+1)\tau} \delta t$ and $\delta\sigma = \delta\chi/\chi_2$. To order $O(\Gamma_1^{-2})$ equations (12a-c) yield $\delta\gamma_1^2 = (\partial_\chi \gamma_1^2) \delta\chi$, $\delta p_1 = (\partial_\chi p_{10}) \delta\chi$, and $\delta\rho_1' = (\partial_\chi \rho_{10}') \delta\chi$. Note that since $\delta\chi \partial_\chi = -\delta t \partial_\tau$ (see (A.1b)) the latter relations simply mean that the Lagrange perturbations of the flow parameters vanish; that is, $\Delta p_1 = \delta p_1 + \delta t \partial_\tau p_{10} = \delta p_1 - (\partial_\chi p_{10}) \delta\chi = 0$, etc. By employing (24a-c) we finally obtain

$$\xi_R(\chi) = 2(m + 1) \partial_\chi \ln g, \quad (39a)$$

$$\xi_p(\chi) = 2(m + 1) \partial_\chi \ln f, \quad (39b)$$

$$\xi_\rho(\chi) = 2(m + 1) \partial_\chi \ln h, \quad (39c)$$

in region 1. Likewise, in region 2 we find, using (18a-c)

$$\eta_R(\chi) = \frac{(m + 1)}{q} \partial_\chi \ln G, \quad (40a)$$

$$\eta_p(\chi) = 2(m + 1) \partial_\chi \ln F, \quad (40b)$$

$$\eta_\rho(\chi) = 2(m + 1) \partial_\chi \ln H. \quad (40c)$$

By direct substitution it can be shown that $\xi_\alpha(\tau, \chi) = \xi_\alpha(\chi) e^{-(m+1)\tau}$, $\eta_\alpha(\tau, \chi) = \eta_\alpha(\chi) e^{-(m+1)\tau}$, with $\xi_\alpha(\chi)$ and $\eta_\alpha(\chi)$ given by (39) and (40), respectively, satisfy the perturbation equations (25), (27), and all the boundary conditions. Note that for this mode $\delta r_{20} = \delta r_2$ in (C.3b) and (C.7e).

The second eigenmode of order $l = 0$ was found by numerically integrating the set of ODEs obtained upon substitution of the relations $\xi_\alpha(\chi, \tau) = \xi_\alpha(\chi) e^{s\tau}$, $\eta_\alpha(\sigma, \tau) = \eta_\alpha(\sigma) e^{s\tau}$ into equations (25) and (27). The method of solution was to guess the eigenvalue s and integrate the equations in each region from the shock to the contact surface. The process was repeated until the condition (36b) was satisfied to the required accuracy. For each choice of parameters we found, using this method, two solutions; the first one coincides with the analytic solution given by (39) and (40). The second one has a smaller decay rate, $s > -(m + 1)$.

4.5 Non-spherical perturbations

For the simulations of non-spherical perturbations ($l \neq 0$) we employed the analytic solution given in (39)-(40) as the initial condition. We have also made some runs for comparison using the second spherical mode found above as the initial condition and verified that the long term evolution of non-spherical growing modes is essentially independent of the details of the initial state. The free parameters of the model are: the indices k and n characterizing the density profiles of the unshocked ambient medium and ejecta (see figure 1), and the adiabatic index $\hat{\gamma}$ of the shocked ejecta. The exponent m and the ratio q are given by (20) and (15), respectively, for a given choice of n , k and $\hat{\gamma}$. Since the reverse shock is non or at best mildly relativistic in the cases examined below we adopt $\hat{\gamma} = 5/3$. We have explored solutions for a range of values of n and k for which m lies in the range 0.5 – 2. The results displayed in figures 3-6 were computed using our canonical choice of parameters: $n = 1.1$, $k = 2$, for which $m = 0.645$, $q = 1.06$. The corresponding unperturbed solution is displayed in figure 2 (left panel). For other values of n and k the solution exhibits the same qualitative behavior, albeit with a larger growth rate for larger values of m . The dependence of the convective growth rate on m is examined in figure 7 and discussed below.

Quite generally we find that eigenmodes having angular scales larger than the causality scale, roughly $l/\Gamma_1 < 1$, decay with time. This is expected since for these modes information can only propagate over distances smaller than the characteristic wavelength, so that a causal section evolves like a spherical mode. An example is shown in figure 3, where solutions obtained for $l(l + 1)/\Gamma_{10}^2 = 0.2$ (upper panels) and

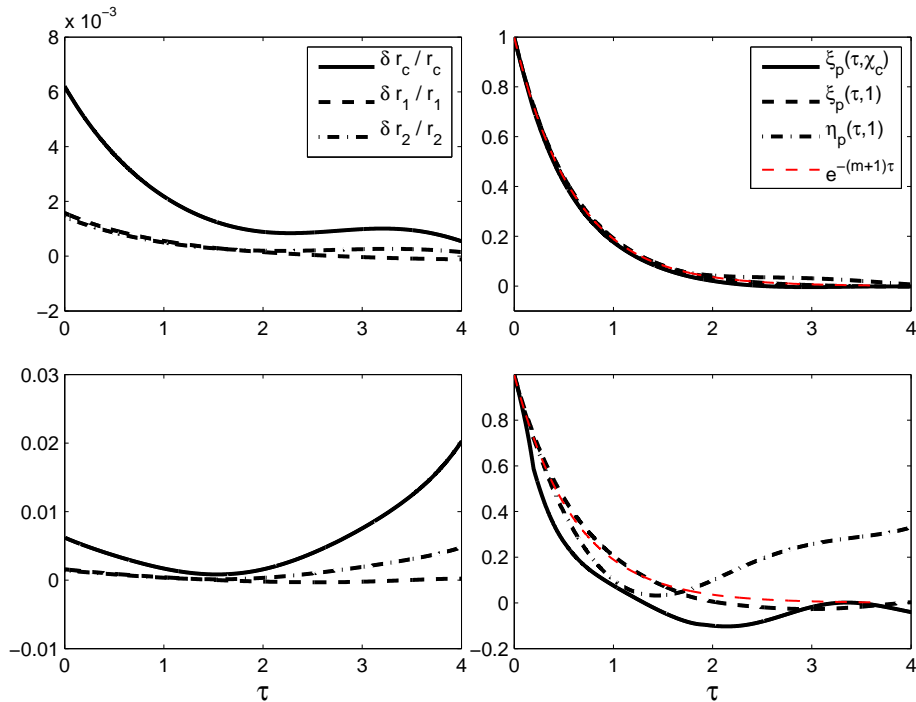


Figure 3. Time evolution of the perturbations for $n = 1.1$, $k = 2$, $l(l+1)/\Gamma_{10}^2 = 0.2$ (upper panels) and $l(l+1)/\Gamma_{10}^2 = 1.5$ (lower panels). Here Γ_{10} being the initial Lorentz factor of the forward shock. The dimensionless distortions of the different surfaces are delineated in the left panels and the relative pressure perturbations (i.e., normalized to their initial values) in the right panels, as indicated. The dashed red line corresponds to the analytic solution of the spherical mode and is plotted here for a comparison.

$l(l+1)/\Gamma_{10}^2 = 1.5$ (bottom panels) are exhibited. Here $\Gamma_{10} = \Gamma_1(\tau = 0)$ denotes the initial Lorentz factor of the forward shock. The analytic solution for the spherical mode is plotted for a comparison in the right panels (dashed red line). The evolution of the dimensionless distortions of the forward and reverse shock fronts, $\delta r_{1(2)}/r_{1(2)} = \delta_{1(2)}/\Gamma_{1(2)}^2$, and the contact surface, $\delta r_c/r_c = \delta_c/\Gamma_c^2$, (see equation (28)) are displayed in the left panels. Relative pressure perturbations are shown in the right panels. The decay of perturbations with an angular scale sufficiently larger than the initial causality scale is evident from this example. The deviation from the analytic solution is small, as seen in the upper right panel. Evolution of longer wavelength modes, $l(l+1)/\Gamma_{10}^2 < 0.2$, is practically identical to that of the spherical mode. The turnover at $\tau \sim 1.5$ exhibited by the solution displayed in the bottom panels is due the fact that $l(l+1)/\Gamma_1^2$ increases with time as $\exp(m\tau)$, so that the wave enters the 'horizon' in this case early enough to affect the evolution of the perturbations at the contact surface. This is roughly the boarder case separating stable and unstable modes.

Modes of order $l > \Gamma_{10}$ are found to be unstable. This is demonstrated in figure 4, where the evolution of an eigenmode of order $l = 10^2 \Gamma_{10}$ is delineated. Oscillations resulting from sound waves crossing, followed by a rapid growth of perturbations in the shocked ejecta and near the contact in the shocked ambient medium are clearly seen. The frequency of oscillations is found to be proportional to the spherical harmonic degree l , as anticipated. Moreover, the frequency of oscillations in region 2 is smaller than that in region 1, owing to the difference in specific enthalpies of the fluids on each side of the contact surface. The growth of perturbations at the contact surface commences very early on, as seen in figure 4. The instability then propagates from the contact to the forward and reverse shocks. The reverse shock responds rather quickly, mainly because it is located much closer to the contact than the forward shock. The propagation of the instability in the shocked ambient medium (region 1) is rather slow, as illustrated in figure 5. The reason is that energy pumped from the contact into this region is now distributed over a much larger volume. However, in reality the instability near the contact will quickly reach the nonlinear regime and saturate, at which point the linear analysis breaks down. What then anticipated is formation of R-T fingers that

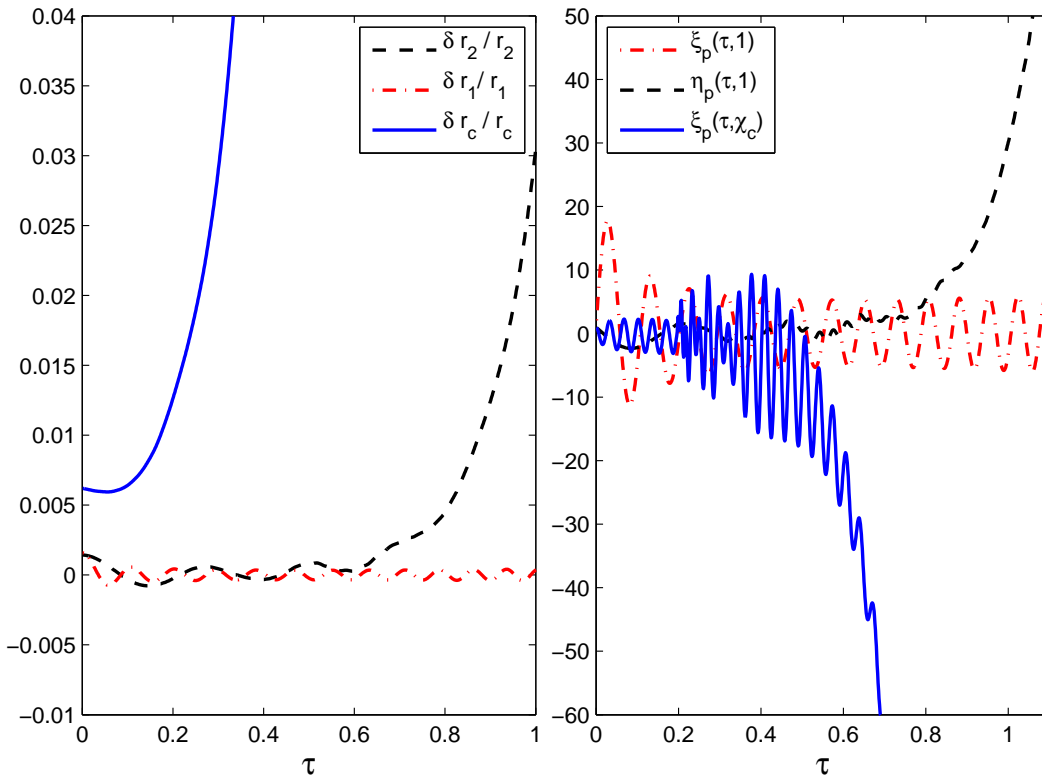


Figure 4. Same as figure 2 but for $l(l+1)/\Gamma_{10}^2 = 10^4$. Left panel: dimensionless distortions of the forward (dotted-dashed line) and reverse (dashed line) shock fronts and the contact surface (solid line). Right panel: relative pressure perturbations at the forward shock front (dotted-dashed line), reverse shock front (dashed line), and the contact surface (solid line).

expand to the forward shock, as seen in the nonrelativistic case (Chevalier *et al.* 1992, Jun and Norman 1996). To study the response of the forward shock requires full, high resolution MHD simulations.

The growth of the perturbations that starts following the decay of the transient initial state is exponential in the time τ , or algebraic in the physical time t , viz. $\delta Q \propto e^{s\tau} \propto (t/t_0)^s$ where Q represents any of the fluid quantities. This is shown in figure 6 for the relativistic distortion δ_c defined in (28). Growth of variables located at larger distances from the contact commences at later times, but follow with the roughly same growth rate. It is also evident from figure 6 that the growth rate s increase with increasing mode degree l . From our numerical simulations we find the scaling $s \propto \sqrt{l/\Gamma_{10}}$, with the proportionality constant depending predominantly on m . Examples are exhibited in figure 7 for two different cases; the first one corresponds to $m = 0.645$ (solid line) and the second one to $m = 2$ (dashed line). A fit to the lines in fig 7 gives $s \simeq \sqrt{l/\Gamma_{10}}$ in the former case and $s \simeq 2.45\sqrt{l/\Gamma_{10}}$ in the latter. This scaling is expected for a R-T instability which is driven by the “effective” gravitational force felt by the decelerating contact interface. To see this, let a_c^μ denotes the 4-acceleration of the contact interface and u_c^μ its 4-velocity. In flat spacetime the acceleration is orthogonal to the velocity, $a^\mu u_\mu = 0$. In the rest frame of the contact $a^\mu = (0, a'_r, 0, 0)$ from which we obtain $a^2 = (a'_r)^2$. From these relations and the normalization of the 4-velocity, $u^2 = 1$, we get $a'_r = du^r/dt \simeq d\Gamma_c/dt = -m\Gamma_c/2t$ for $\Gamma_c^2 \propto (t/t_0)^{-m}$. The “effective” gravitational force felt by the decelerating contact is just $g = -a'_r$. Now, the wavevector component parallel to the contact surface, $k_{||}$, is given roughly by $k_{||} = r_c/l$ for an eigenmode of order l . We thus have $\sqrt{gk_{||}}t' \simeq \sqrt{ml/2\Gamma_c} \propto s$, noting that $t' = t/\Gamma_c$ and that the ratio Γ_c/Γ_1 is independent of time. Consequently, the growth rate, as measured in the rest frame of the contact, is $s/t' \propto \sqrt{gk_{||}}$, which is just the R-T growth rate in the case $\rho_{2c} \gg \rho_{1c}$. Note that the dependence of s on m , as derived from the simulations, reflects not only the effect of deceleration but also the dependence of the unperturbed solution on m , in particular the density ratio

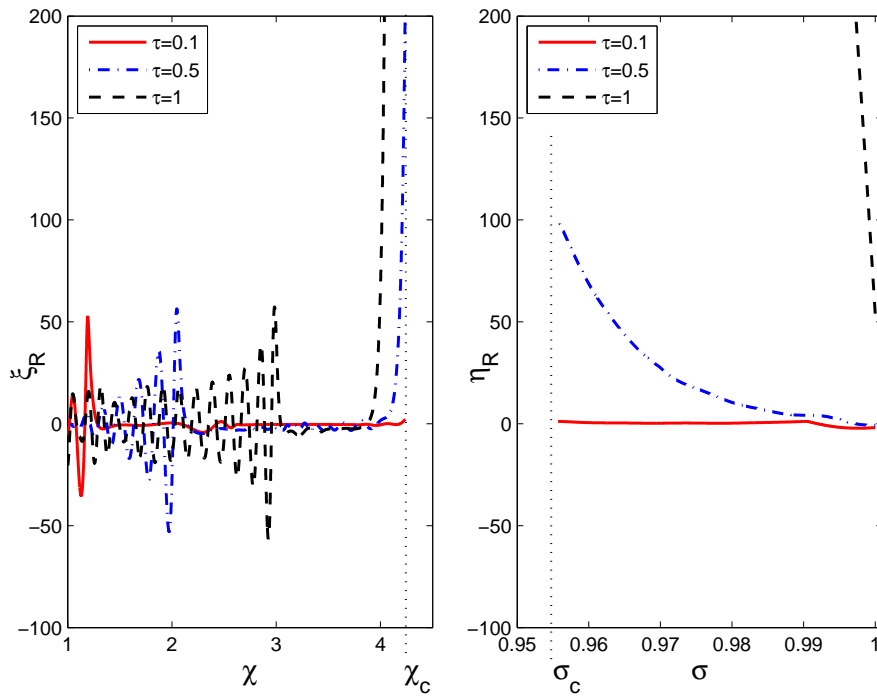


Figure 5. Profile of the dimensionless perturbation of radial velocity at different times. Left panel: shocked ambient medium (region 1). The location of the forward shock is at $\chi = 1$. The location of the contact discontinuity χ_c is indicated. Rapid growth of the perturbation near the contact is clearly seen. The wave propagating from the forward shock to the contact interface corresponds to transmission of the initial shock disturbance. Right panel: shocked ejecta (region 2). Here η_R is plotted against the normalized variable $\sigma = \chi/\chi_2$ (see equation (16)). The locations of the reverse shock and the contact discontinuity are at $\sigma = 1$ and $\sigma = \sigma_c = \chi_c/\chi_2$, respectively. As seen, at $\tau = 1$ the instability already propagated throughout the entire region.

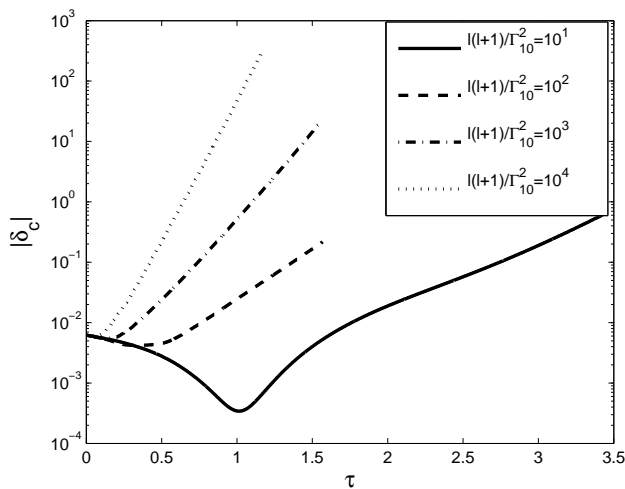


Figure 6. Absolute value of the relativistic distortion δ_c defined in equation (28) (see also (36c)) versus time τ , for different values of the spherical harmonic degree l .

at the contact, as can be seen from figure 2.

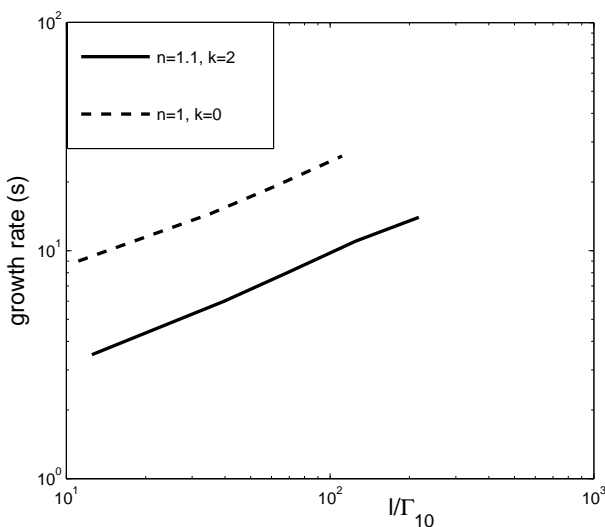


Figure 7. Dimensionless growth rate versus l/Γ_{10} . The solid line corresponds to $m = 0.645$ and the dashed line to $m = 2$.

5 Implications for GRBs

In the standard GRB model the afterglow emission observed following the explosion is commonly attributed to synchrotron cooling of relativistic electrons behind the forward shock (Meszaros and Rees 1997) (but c.f., (Lucas and Beloborodov 2007, Genet *et al.* 2007)). The observations seem to indicate the presence of strong magnetic fields over a significant portion of the shocked circumburst layer. The magnetic energy density estimated from the data, roughly a fraction $\epsilon_B \sim 10^{-3} - 10^{-1}$ of the internal energy density (Panaitescu and Kumar 2002), is several orders of magnitudes larger than that expected from compression of the preshock magnetic field. This implies magnetic field generation or amplification by some mechanism. Whether kinetic processes can generate such magnetic fields is yet an open issue. Plasma instabilities that develop in the collisionless shock transition generate strong magnetic fields on kinetic scales. However, recent shock simulations (Spitkovsky 2008) indicate that the fields thereby produced decay rapidly over a few skin depths, before reaching the MHD scale. Magnetic field generation by streaming ultra-relativistic protons (or cosmic rays) in the immediate shock upstream has also been considered. In this scenario the magnetized cosmic ray precursor is envisioned to form as an inherent part of the shock transition. The key question here is whether the shock can indeed inject enough energy in the form of ultra-relativistic particles to sustain the required large scale magnetic field. To study this process using self-consistent shock simulations requires computing time beyond present capabilities.

An alternative to plasma instabilities is magnetic field amplification by MHD turbulence. It has been proposed (Sironi and Goodman 2007) that macroscopic turbulence might be produced via the interaction of the forward shock with a clumpy circumburst medium. In this scenario the response of the shock to the preshock density inhomogeneities leads to generation of vorticity and the consequent amplification of magnetic fields (Zhang *et al.* 2009). Amplification of magnetic energy to the level inferred from observations requires large (order unity) density contrasts and filling factors of the clumps. Whether such conditions exist in the surrounding environment is yet an open issue. Here we propose that the convective instability found above may be an inherent source of turbulence in the shocked circumburst layer, at least at early times. The instability may also lead to nonlinear distortions of the shock front itself without the need for an external driver. If the ejecta is magnetized at a level smaller than that required to suppress the instability but still much larger than that of the unshocked ambient medium, then mixing of the magnetized ejecta with the shocked ambient gas via growth of R-T fingers alone can lead to strong magnetization of shocked circumburst layer at sufficiently early times. How the system evolves at later times, after the reverse shock crosses the ejecta, is unclear at present. The stability analysis of the BMK solution performed by Gruzinov (2000) suggests that it may be a very slow attractor. Linear perturbations of the forward shock in the BMK phase decay very slowly. Whether this behavior persists also in the nonlinear regime is yet to be

determined. If it does then it could well be that the growth of R-T fingers and, perhaps, the nonlinear oscillations of the forward shock itself which are induced by the convective instability may be a source of vorticity during a long portion of the evolution of the blast wave (Milosavljevic and Nakar 2007). The simulations performed by Zhang et al. (2009) suggest a saturation level of $\epsilon_B \sim 5 \times 10^{-3}$ for the turbulence induced magnetic energy density, weakly dependent on the initial magnetic field strength.

The convective instability may also affect the emission from the shocked ejecta. As shown above, the effect of the instability on the reverse shock is prompt and dramatic. The nonlinear distortions of the reverse shock may strongly alter particle acceleration and the emission processes during reverse shock crossing. It is tempting to speculate that the lack of observed optical flashes, that are anticipated in the “standard” model, and the behavior of the early afterglow phase may be attributed to the instability discussed here, although we do not offer at present any specific explanation. At any rate, the salient lesson is that a careful analysis that takes account of this process is required to better understand the observational characteristics of the emission during the early post-prompt phase.

6 Summary

We have performed a global linear stability analysis of a self-similar solution describing the interaction of a relativistic shell with an ambient medium. Our analysis indicates a strong convective instability at early stages of the evolution of the dense ejecta as it sweeps a lighter ambient gas. Our main findings are:

1. Eigenmodes having angular scales smaller than the causality scale, roughly $l/\Gamma_1 > 1$, where Γ_1 is the Lorentz factor of the blast wave, are unstable and exhibit a rapid growth. Lower order modes for which $l/\Gamma_1 < 1$ are stable.

2. Growth of perturbations starts promptly near the contact discontinuity. The instability then propagates towards the forward and reverse shocks. The reverse shock responds quickly to the growth of distortions at the contact. Propagation of the signal to the forward shock is much slower. The instability near the contact becomes nonlinear well before the signal arrives at the forward shock, so full MHD simulations are needed to resolve the effect of the instability on the forward shock.

3. The growth is algebraic in time, that is, $\delta Q \propto (t/t_0)^s$ for any fluid quantity Q . The dimensionless growth rate scales as $s \propto \sqrt{l/\Gamma_1}$, with a proportionality constant that increases with increasing m . This implies development of a very small scale structure with a significant amplitude, up to the dissipation scale, at least at sufficiently early times. The effect of such corrugations on the collisionless shock transition and related processes, particularly particle acceleration, needs to be explored.

Unfortunately, the linear analysis outlined above is restricted to a limited set of conditions under which the unperturbed self-similar solution of Nakamura & Shigeyama (2006) is applicable. It is naively expected that the instability will be strongly suppressed in cases where the ejecta is highly magnetized and/or if the reverse shock is highly relativistic. Full 3D MHD simulations should be exploited to study this process in other situations, and to follow the evolution of the convective instability in the nonlinear regime. As illustrated above, high resolution simulations that can resolve angular scales $\Delta\theta \ll 1/\Gamma$ are required, posing a great numerical challenge. We believe that our findings strongly motivate such efforts.

I thank A. D itkowski for a technical help in the development of the code, and M. Aloy, D. Kushnir, M. Lyutikov, A. MacFadyen, E. Nakar and E. Waxman for enlightening discussions. This work was supported by an ISF grant for the Israeli Center for High Energy Astrophysics, and by the NORDITA program on Physics of relativistic flows.

Appendix A

Derivation of the unperturbed flow equations

A.1 Region 1

The derivation of the flow equations in region 1 (the shocked ambient medium) is straightforward and follows that in Blandford and McKee (1976). Transforming from the coordinates (r, t) to (χ, τ) , with $\tau = \ln t$ and χ given by (8), and using the relations

$$t\partial_t = \partial_\tau + [(m+1)(2\Gamma_1^2 - \chi) + 1]\partial_\chi, \quad (\text{A.1a})$$

$$t\partial_r = -[1 + 2(m+1)\Gamma_1^2]\partial_\chi, \quad (\text{A.1b})$$

$$td_t^0 = \partial_\tau + (m+1)(2/g - \chi)\partial_\chi, \quad (\text{A.1c})$$

one obtains, upon substitution of equations (12a-c) into the flow equations (3a,b),

$$\frac{1}{g} \frac{d \ln g}{d\chi} = \frac{(7m+3k-4) - (m+2)g\chi}{(m+1)(4-8g\chi+g^2\chi^2)}, \quad (\text{A.2a})$$

$$\frac{1}{g} \frac{d \ln f}{d\chi} = \frac{8(m-1) + 4k - (m+k-4)g\chi}{(m+1)(4-8g\chi+g^2\chi^2)}, \quad (\text{A.2b})$$

$$\frac{1}{g} \frac{d \ln h}{d\chi} = \frac{2(9m+5k-8) - 2(5m+4k-6)g\chi + (m+k-2)g^2\chi^2}{(m+1)(4-8g\chi+g^2\chi^2)(2-g\chi)}. \quad (\text{A.2c})$$

A.2 Region 2

In region 2 we use the coordinates (τ, σ) . Then,

$$t\partial_t = \partial_\tau + [(m+1)(2\Gamma_2^2 - \sigma) + 1]\partial_\sigma, \quad (\text{A.3a})$$

$$t\partial_r = -[1 + 2(m+1)\Gamma_2^2]\partial_\sigma, \quad (\text{A.3b})$$

$$td_t^0 = \partial_\tau + (m+1)(1/qG - \sigma)\partial_\sigma. \quad (\text{A.3c})$$

Substituting (18a-c) into equations (3a,b) yields

$$2(1+qG\sigma)\frac{d \ln F}{d\sigma} - (1-qG\sigma)\kappa\frac{d \ln G}{d\sigma} = \frac{(mn - \kappa m - 6)}{(m+1)}qG, \quad (\text{A.4a})$$

$$2(1-qG\sigma)\frac{d \ln F}{d\sigma} - \hat{\gamma}(1+qG\sigma)\frac{d \ln G}{d\sigma} = \frac{[\hat{\gamma}(m+2) - mn - 6(\hat{\gamma}-1)]}{(m+1)}qG, \quad (\text{A.4b})$$

$$2(1-qG\sigma)\frac{d \ln H}{d\sigma} - 2\frac{d \ln G}{d\sigma} = -\frac{(mn - m - 2)}{(m+1)}qG, \quad (\text{A.4c})$$

where $\kappa(\sigma) = W_2/p_2\gamma_2^2$, and $\hat{\gamma}$ denotes the adiabatic index.

Appendix B

Derivation of the equations for the dimensionless perturbations

B.1 Region 1

To derive the equations for the dimensionless perturbations $\xi_\alpha(\tau, \chi)$ we first write equations (23a-d) in the new coordinates (χ, τ) , using the relations (A.1a-c) and (24a-d). Recalling that $W_1 = 4p_1\gamma_1^2$ and noting that $r\nabla\delta\mathbf{v}_{1T} = -l(l+1)\xi_T Y_{l\bar{m}}$, we obtain from the continuity equation (23a)

$$\partial_\tau \xi_\rho + (m+1)(2/g - \chi)\partial_\chi \xi_\rho - \frac{2(m+1)}{g}\partial_\chi \xi_R + \frac{2(m+1)}{g}(\partial_\chi \ln g - \partial_\chi \ln h)\xi_R = l(l+1)\xi_T. \quad (\text{B.1a})$$

Equation (23b) gives

$$\begin{aligned} \partial_\tau(\xi_P + \frac{2}{3}\xi_R) + \frac{(m+1)}{g}[(2 - g\chi)\partial_\chi \xi_P - \frac{2}{3}(2 + g\chi)\partial_\chi \xi_R] \\ + \frac{2(m+1)}{g}[\frac{2}{3}\partial_\chi \ln g - \partial_\chi \ln f]\xi_R = \frac{4}{3}l(l+1)\xi_T, \end{aligned} \quad (\text{B.1b})$$

the transverse component of the momentum equation (23c) gives

$$\partial_\tau \xi_T + (m+1)(2/g - \chi)\partial_\chi \xi_T + [(m+1)(2/g - \chi)\partial_\chi \ln(fg/h) - m]\xi_T = -\frac{\xi_P}{2g\Gamma^2}, \quad (\text{B.1c})$$

and the energy equation (23d) gives

$$\partial_\tau(\xi_P + 2\xi_R) + 2(m+1)(2/g - \chi)\partial_\chi \xi_R - (m+1)(2/g + \chi)\partial_\chi \xi_P + c_{oR}\xi_R + c_{oP}\xi_P = 0, \quad (\text{B.1d})$$

where

$$c_{oR} = -(3m+k) - (m+1)\chi\partial_\chi[2(\ln g) + (\ln f)], \quad (\text{B.2a})$$

$$c_{oP} = -(3m+k) + 2(m+1)(2/g - \chi)\partial_\chi(\ln g) - (m+1)(2/g + \chi)\partial_\chi(\ln f). \quad (\text{B.2b})$$

Note that (B.1c) holds only for $l \neq 0$. In this case it is readily seen from (B.1b,c) that ξ_P and ξ_T must have different time evolution, owing to the extra factor Γ^{-2} on the right-hand side of (B.1c), implying breakdown of self-similarity. In the spherical case ($l = 0$), $\nabla_T Y_{l\bar{m}} = 0$, and equation (23c) is identically zero. The right-hand sides of (B.1a,b) then vanishes allowing separation of variables.

For an impulsive BMK76 solution with $k = 0$, $m = 3$, $g = \chi^{-1}$, $h = \xi^{-7/4}$ and $f = \chi^{-17/12}$ the above equations reduce to

$$\partial_\tau \xi_\rho + 4\chi\partial_\chi \xi_\rho - 8\chi\partial_\chi \xi_R + 6\xi_R = l(l+1)\xi_T, \quad (\text{B.3a})$$

$$\partial_\tau[\xi_P + (2/3)\xi_R] + 4\chi\partial_\chi \xi_P - 8\chi\partial_\chi \xi_R + 6\xi_R = \frac{4}{3}l(l+1)\xi_T, \quad (\text{B.3b})$$

$$\partial_\tau \xi_T + 4\chi\partial_\chi \xi_T - \frac{17}{3}\xi_T + \frac{\xi_P}{2g\Gamma^2} = 0, \quad (\text{B.3c})$$

$$\partial_\tau(\xi_P + 2\xi_R) + 8\chi\partial_\chi \xi_R - 12\chi\partial_\chi \xi_P + \frac{14}{3}\xi_R = 0, \quad (\text{B.3d})$$

as derived originally by Gruzinov (2000) (except for the 3rd term on the right-hand side of (B.3c), see footnote at the end of section 4.3). After some manipulation of equations (B.1a-d) we arrive at (25), with

the different coefficients given by

$$A_{RR} = A_{PP} = (m+1)(\chi - 4/g), \quad (\text{B.4a})$$

$$A_{PR} = \frac{4}{3}A_{RP} = 2A_{\rho R} = \frac{4(m+1)}{g}, \quad (\text{B.4b})$$

$$A_{\rho\rho} = A_{TT} = -(m+1)(2/g - \chi), \quad (\text{B.4c})$$

and

$$B_{RR} = \frac{3(3m+k)}{4} + \frac{(m+1)}{2} \left(\frac{2}{g} + 3\chi \right) \partial_\chi \ln g - \frac{3(m+1)}{4} \left(\frac{2}{g} - \chi \right) \partial_\chi \ln f, \quad (\text{B.5a})$$

$$B_{PR} = -\frac{(3m+k)}{2} - (m+1) \left(\frac{2}{g} + \chi \right) \partial_\chi \ln g + \frac{(m+1)}{2} \left(\frac{6}{g} - \chi \right) \partial_\chi \ln f, \quad (\text{B.5b})$$

$$B_{PP} = -\frac{3}{2}B_{RP} = -\frac{(3m+k)}{2} + (m+1) \left(\frac{2}{g} - \chi \right) \partial_\chi \ln g - \frac{(m+1)}{2} \left(\frac{2}{g} + \chi \right) \partial_\chi \ln f, \quad (\text{B.5c})$$

$$B_{PT} = -2B_{RT} = 2B_{\rho T} = 2l(l+1), \quad (\text{B.5d})$$

$$B_{\rho R} = -\frac{2(m+1)}{g} \partial_\chi \ln(g/h), \quad (\text{B.5e})$$

$$B_{TP} = -1/(2g\Gamma^2), \quad (\text{B.5f})$$

$$B_{TT} = m - (m+1) \left(\frac{2}{g} - \chi \right) \partial_\chi \ln(fg/h). \quad (\text{B.5g})$$

All other coefficients vanish.

B.2 Region 2

The derivation of the perturbation equations in region 2 is similar to that in region 1, but slightly more involved. Here we express (23a-d) in the coordinates (σ, τ) , using the relations (A.3a-c) and (26a-d). To shorten the notation we define $a = \hat{\gamma}/(\hat{\gamma} - 1)$ and $\Delta_\pm = (m+1)(1/qG \pm \sigma)$. From the continuity equation (23a) we then obtain

$$\partial_\tau \eta_\rho + \Delta_- \partial_\sigma \eta_\rho - \frac{2(m+1)}{G} \partial_\sigma \eta_R + \frac{2(m+1)}{G} (\partial_\sigma \ln G - \partial_\sigma \ln H) \eta_R = l(l+1) \eta_T, \quad (\text{B.6a})$$

noting that $r \nabla \delta \mathbf{v}_{2T} = -l(l+1) \eta_T Y_{l\tilde{m}}$. Likewise, (23b) yields

$$\partial_\tau \eta_T + \Delta_- \partial_\sigma \eta_T + \left[\frac{a}{\kappa} \Delta_- \partial_\sigma \ln(F/H) + \frac{\kappa+a}{2\kappa} \Delta_- \partial_\sigma \ln G - m/2 \right] \eta_T + \frac{\eta_P}{\kappa q G \Gamma_2^2} = 0, \quad (\text{B.6b})$$

where the relation $W_{20}/p_{20} = \kappa q G \Gamma_2^2$ has been used, the transverse component of the momentum equation (23c) gives

$$\partial_\tau (\eta_P + \hat{\gamma} q \eta_R) + \Delta_- \partial_\sigma \eta_P - \hat{\gamma} q \Delta_+ \partial_\sigma \eta_R + \frac{(m+1)}{G} [\hat{\gamma} \partial_\sigma \ln G - 2 \partial_\sigma \ln F] \eta_R = \hat{\gamma} l(l+1) \eta_T, \quad (\text{B.6c})$$

and (23d) gives

$$\kappa q \partial_\tau \eta_R + \partial_\tau \eta_P + \kappa q \Delta_- \partial_\sigma \eta_R - \Delta_+ \partial_\sigma \eta_P + c_{iR} \eta_R + c_{iP} \eta_P + c_{i\rho} \eta_\rho = 0, \quad (\text{B.6d})$$

with

$$c_{i\rho} = -c_{i\rho} = \frac{\kappa - a}{2}(-m + \Delta_- \partial_\sigma \ln G), \quad (\text{B.7a})$$

$$c_{iR} = \frac{2(m+1)}{G} \partial_\sigma \ln F - \kappa \frac{(m+1)}{G} \partial_\sigma \ln G - qc_{i\rho}. \quad (\text{B.7b})$$

After some algebra equations (B.6a-d) can be recast into the form of (27), with the coefficients $C_{\alpha\beta}$, $D_{\alpha\beta}$ given explicitly by:

$$C_{RR} = C_{PP} = (m+1) \left[\sigma - \frac{\kappa + \hat{\gamma}}{qG(\kappa - \hat{\gamma})} \right], \quad (\text{B.8a})$$

$$C_{RP} = \frac{1}{q^2 \hat{\gamma} \kappa} C_{PR} = \frac{2(m+1)}{q^2 G(\kappa - \hat{\gamma})}, \quad (\text{B.8b})$$

$$C_{\rho R} = \frac{2(m+1)}{G}, \quad (\text{B.8c})$$

$$C_{\rho\rho} = C_{TT} = (m+1)(\sigma - 1/qG), \quad (\text{B.8d})$$

and

$$D_{RR} = \frac{(m+1)}{qG(\kappa - \hat{\gamma})} [-4\partial_\sigma \ln F + (\kappa + \hat{\gamma})\partial_\sigma \ln G] + \frac{\kappa - a}{2(\kappa - \hat{\gamma})} [\Delta_- \partial_\sigma \ln G - m], \quad (\text{B.9a})$$

$$D_{PR} = \frac{2(m+1)}{G(\kappa - \hat{\gamma})} [(\hat{\gamma} + \kappa)\partial_\sigma \ln F - \kappa \hat{\gamma} \partial_\sigma \ln G] - \frac{q\hat{\gamma}(\kappa - a)}{2(\kappa - \hat{\gamma})} [\Delta_- \partial_\sigma \ln G - m], \quad (\text{B.9b})$$

$$D_{PP} = -q\hat{\gamma}D_{RP} = -\frac{\hat{\gamma}(\kappa - a)}{2(\kappa - \hat{\gamma})} [\Delta_- \partial_\sigma \ln G - m], \quad (\text{B.9c})$$

$$D_{PT} = -q\kappa D_{RT} = \frac{\hat{\gamma}\kappa l(l+1)}{(\kappa - \hat{\gamma})q}, \quad (\text{B.9d})$$

$$D_{\rho R} = \frac{2(m+1)}{G} \partial_\sigma \ln(G/H), \quad (\text{B.9e})$$

$$D_{\rho T} = l(l+1), \quad (\text{B.9f})$$

$$D_{TP} = -\frac{1}{\kappa q \Gamma_2^2 G}, \quad (\text{B.9g})$$

$$D_{TT} = -\frac{a}{\kappa} \Delta_- \partial_\sigma \ln(F/H) - \frac{\kappa + a}{2\kappa} \Delta_- \partial_\sigma \ln G + m/2. \quad (\text{B.9h})$$

Appendix C

Boundary conditions at the reverse shock

The normal to the reverse shock is written $n_{2\mu} = n_{2\mu}^0 + \delta n_{2\mu}$, where $n_{2\mu}^0$ and $\delta n_{2\mu}$ are given by equations (31a,b), respectively, with the subscript 1 replaced by 2. Applying (30a) to the reverse shock we have

$$\rho'_{20} v_{20}^\mu \delta n_{2\mu} + (\Delta_2 \rho'_{20} v_{20}^\mu + \rho'_{20} \Delta_2 v_{20}^\mu) n_\mu^0 = \rho'_e v_e^\mu \delta n_{2\mu} + (\Delta_2 \rho'_e v_e^\mu + \rho'_e \Delta_2 v_e^\mu) n_\mu^0, \quad (\text{C.1})$$

with the density of the unshocked ejecta ρ_e is given by (7), $v_e^\mu = (1, v_e, 0, 0)$, etc. The velocity of the unshocked ejecta near the shock surface evolves with time as $dv_e/dt = \partial_t v_e + (V_2 + \delta V_2) \partial_r v_e$. Integrating over time from $t = t_0$ we find $\Delta_2 v_e = (\delta r_2/t)(1 - \delta r_{20}/\delta r_2)$ to the order to which we are working,

where δr_{20} is the initial displacement of the reverse shock surface. From (28) we then obtain $\Delta_2 v_e^\mu n_{2\mu}^0 = (1 - \delta r_{20}/\delta r_2)(\delta_2/\Gamma_2)Y_{l\bar{m}}$. The corresponding convective change of the density ρ_e' is $\Delta_2 \ln \rho_e' = (1 - n)(m + 1)\Gamma_2^2 \Delta_2 v_e$. Using (31b) with the subscript 1 replaced by 2 we also have $2(m+1)v_e^\mu \delta n_{2\mu} = -(m+2)\Gamma_2 \delta V_2 Y_{l\bar{m}}$. For the perturbations of the shocked ejecta we obtain, using the unperturbed flow parameters (18a-c), $\Delta_2 \ln \rho_e' = [\eta_\rho - 2(m+1)\delta_2 \partial_\sigma(\ln H)_2]Y_{l\bar{m}}$, and $q\Gamma_2^2 \Delta_2 v_2 = [q\eta_R - (m+1)\delta_2 \partial_\sigma(\ln G)_2]Y_{l\bar{m}}$. Substituting the above results into (C.1) yields

$$\partial_\tau \delta_2 + A_{sR}\eta_R + A_{s\rho}\eta_\rho + A_{s\delta}\delta_2 = 0, \quad (\text{C.2})$$

where

$$A_{sR} = \frac{2q}{q-1}A_{s\rho} = \frac{qm}{q-m-1}, \quad (\text{C.3a})$$

$$A_{s\delta} = m+1 - \frac{m(m+1)}{(q-m-1)}\{\partial_\sigma(\ln G)_2 + (q-1)\partial_\sigma(\ln H)_2\} \\ - \frac{(m+1)(m+2-mn)(q-1)}{2(q-m-1)}(1 - \delta r_{20}/\delta r_2). \quad (\text{C.3b})$$

The transverse component of (30b) reduces to

$$\eta_T = \frac{2}{\kappa(q-1)}\frac{\delta_2}{\Gamma_2^2}, \quad (\text{C.4})$$

and the zeroth component reads

$$W_{20}v_{20}^\mu \delta n_{2\mu} + (\Delta_2 W_2 v_{20}^\mu + W_{20}\Delta_2 v_2^\mu)n_{2\mu} - (p_{20}\delta n_{20} + \Delta_2 p_2 n_{20}) = \\ W_e v_e^\mu \delta n_{2\mu} + (\Delta_2 W_e v_e^\mu + W_e \Delta_2 v_e^\mu)n_{2\mu}, \quad (\text{C.5})$$

with $W_e = \rho_e \gamma_e^2$, $\Delta_2 W_e = \rho_e \gamma_e^2(2-n)(m+1)\delta_2(1 - \delta r_{20}/\delta r_2)Y_{l\bar{m}}$, $\Delta_2 W_2 = p_{20}(\kappa + a)q^2(\Gamma_4^2 \Delta v_2) + q(\kappa - a)\Delta \ln \rho_e' + qa\Delta_2 \ln p_2$, and $\Delta_2 \ln p_2 = [\eta_P - 2(m+1)\delta_2 \partial_\sigma(\ln F)_2]Y_{l\bar{m}}$. Rearranging terms we finally arrive at

$$B_{st}\partial_\tau \delta_2 + B_{s\delta}\delta_2 + B_{sR}\eta_R + B_{sP}\eta_P + B_{s\rho}\eta_\rho = 0, \quad (\text{C.6})$$

where

$$B_{st} = 1 - \frac{q+1}{2}\kappa + \frac{m+2}{2}\frac{\rho_e}{P_{20}}, \quad (\text{C.7a})$$

$$B_{sR} = \frac{q(q+1)}{2}(\kappa - a) + aq^2, \quad (\text{C.7b})$$

$$B_{sP} = \frac{a(q-1) + 2}{2}, \quad (\text{C.7c})$$

$$B_{s\rho} = \frac{q-1}{2}(\kappa - a), \quad (\text{C.7d})$$

$$B_{s\delta} = (m+1) \left[B_{st} - \frac{B_{sR}}{q}\partial_\sigma(\ln G) - 2B_{sP}\partial_\sigma(\ln F) - 2B_{s\rho}\partial_\sigma(\ln H) \right] \\ + \frac{\rho_e}{P_{20}}(m+1)(mn/2 - m - 1)(1 - \delta r_{20}/\delta r_2). \quad (\text{C.7e})$$

Subtracting the radial component of (30b) from (C.5) we obtain

$$[W_{20}v_{20}^\mu \delta n_{2\mu} + (\Delta_2 W_2 v_{20}^\mu + W_{20} \Delta_2 v_2^\mu) n_{2\mu}^0](v_{20} - v_e) + W_{20}(\Delta_2 v_2) v_{20}^\mu n_{2\mu}^0 + p_{20}(V_2 - v_e) \Gamma_2^3 \delta V_2 + \Delta_2 p_2 (1 - V_2 v_e) \Gamma_2 = W_e (\Delta_2 v_e) v_e^\mu n_{2\mu}^0, \quad (\text{C.8})$$

whereby the final condition,

$$C_{st} \partial_\tau \delta_2 + C_{s\delta} \delta_2 + C_{sR} \eta_R + C_{sP} \eta_P + C_{s\rho} \eta_\rho = 0, \quad (\text{C.9})$$

is derived, with

$$C_{st} = \frac{(m+1-q)(q+1)\kappa}{2q} - m, \quad (\text{C.10a})$$

$$C_{sR} = \frac{(q-m-1)}{2} [(q+1)\kappa + (q-1)a] + (q-1)(m+1)\kappa, \quad (\text{C.10b})$$

$$C_{sP} = \frac{(q-m-1)(q-1)}{2q} a + (m+2), \quad (\text{C.10c})$$

$$C_{s\rho} = \frac{(q-m-1)(q+1)}{2q} (\kappa - a), \quad (\text{C.10d})$$

$$C_{s\delta} = (m+1) \left[C_{st} - \frac{C_{sR}}{q} \partial_\sigma (\ln G) - 2C_{sP} \partial_\sigma (\ln F) - 2C_{s\rho} \partial_\sigma (\ln H) \right]. \quad (\text{C.10e})$$

With the exception of the spherical mode associated with a linear time translation of the solution outlined in section 3, for which $\delta V_2 = 0$ and $\delta r_2(t) = \delta r_{20}$ (see section 4.4), we shall assume $\delta r_{20} = 0$. We can then eliminate δ_2 from (C.2), (C.4), (C.6) and (C.9) to obtain equations (34a-d), where we define

$$d_{s\alpha} = \frac{C_{s\alpha} B_{st} - B_{s\alpha} C_{st}}{C_{s\delta} B_{st} - B_{s\delta} C_{st}}; \quad \alpha = (R, P, \rho), \quad (\text{C.11a})$$

$$e_{s\alpha} = -\frac{C_{s\alpha} B_{s\delta} - B_{s\alpha} C_{s\delta}}{C_{s\delta} B_{st} - B_{s\delta} C_{st}}; \quad \alpha = (R, P, \rho), \quad (\text{C.11b})$$

$$f_{s\lambda} = \frac{B_{s\lambda} - A_{s\lambda} B_{st}}{B_{s\rho} - A_{s\rho} B_{st}}; \quad \lambda = (R, P, \delta). \quad (\text{C.11c})$$

Appendix D

Equations for the Riemann invariants

Define the vector $|\xi\rangle = (\xi_R, \xi_P, \xi_\rho, \xi_T)$. Then (25) can be expressed in matrix notation as

$$\partial_\tau |\xi\rangle = A \partial_\sigma |\xi\rangle + B |\xi\rangle, \quad (\text{D.1})$$

with $A(\chi)$ and $B(\chi)$ denoting the matrices $(A_{\alpha\beta})$ and $(B_{\alpha\beta})$, respectively. Let $|\psi_q\rangle$; $q = (+, -, 3, 4)$ be the eigenvectors of A and λ_q the corresponding eigenvalues. We find

$$\lambda_\pm = A_{RR} \pm \frac{\sqrt{3}}{2} A_{PR}, \quad (\text{D.2a})$$

$$\lambda_3 = \lambda_4 = -(m+1)(2/g - \chi), \quad (\text{D.2b})$$

$$(\text{D.2c})$$

where A_{RR} and A_{PR} are given by (B.4a,b) respectively. The Riemann invariants in region 1, given explicitly in (37), are the coefficients of the expansion of $|\xi\rangle$ in the basis vectors $|\psi_q\rangle$, that is, $|\xi\rangle = \Sigma_q \xi_q |\psi_q\rangle$. They obey the equations

$$\partial_\tau \xi_q = \lambda_q \partial_\chi \xi_q + \Sigma_p R_{qp} \xi_p, \quad (\text{D.3})$$

where $R_{qp} = \langle \psi_q | B | \psi_p \rangle$. We find that $\lambda_-, \lambda_3, \lambda_4$ are negative everywhere in region 1, whereas λ_+ is positive, so that ξ_-, ξ_3, ξ_4 propagate from the forward shock to the contact while ξ_+ propagates in the opposite direction.

The analysis in region 2 is similar but slightly more complicated, as the eigenvectors $|\zeta_p\rangle$ of the matrix C , the elements of which are given in (B.8a-d), depend on the self-similarity parameter σ . The Riemann invariants defined in (38) were computed using the relation $|\eta\rangle = \Sigma_q \eta_q |\zeta_q\rangle$, where $|\eta\rangle = (\eta_R, \eta_P, \eta_\rho, \eta_T)$. For the eigenvalues of the matrix C we have

$$\tilde{\lambda}_\pm = C_{RR} \pm \frac{C_{PR}}{q\sqrt{\kappa\gamma}}, \quad (\text{D.4a})$$

$$\tilde{\lambda}_3 = \tilde{\lambda}_4 = -(m+1)(1/qG - \sigma). \quad (\text{D.4b})$$

The equation governing the evolution of the Riemann invariants in this region reads:

$$\partial_\tau \eta_q = \tilde{\lambda}_q \partial_\chi \eta_q + \Sigma_p T_{qp} \eta_p, \quad (\text{D.5})$$

where $T_{qp} = \langle \zeta_q | D | \zeta_p \rangle + \langle \zeta_q | C | \partial_\sigma \zeta_p \rangle$. The eigenvalues $\tilde{\lambda}_+, \tilde{\lambda}_3, \tilde{\lambda}_4$ are positive everywhere while $\tilde{\lambda}_-$ is negative hence η_+, η_3, η_4 propagate from the reverse shock to the contact while η_- propagates from the contact to the reverse shock.

REFERENCES

- Blandford, R. D. and McKee, C. F. "Fluid dynamics of relativistic blast wave," *Phys. Fluids*, 1976, **19**, 1130
- Chevalier R. A., Blondin, J. M. and R. Emmering "Hydrodynamic instabilities in supernova remnants: self-similar driven waves," *Astrophys. J.*, 1992, **392**, 118
- Genet, F. Daigne F. and Mochkovitch, R. "Can the early X-ray afterglow of gamma-ray bursts be explained by a contribution from the reverse shock?" *Monthly Not. Royal Astron. Soc.*, 2007, **381**, 732
- Giannios D. and Spruit, H. C. "Spectra of Poynting-flux powered GRB outflows," *Astron. Astrophys.*, 2005, **430**, 1
- Giannios D., Mimica, P. and Aloy, M. A., "On the existence of a reverse shock in magnetized gamma-ray burst ejecta" *Astronomy and Astrophysics*, 2008, **478**, 747
- Goodman, J. and MacFadyen, A. "Ultra-relativistic geometrical shock dynamics and vorticity," *J. Fluid Mechanics*, 2008, **604**, 325
- Gruzinov, A. "Ultra-relativistic blast waves: stability and strong non-universality," *arXiv:astro-ph/0012364*, 2000
- Gull, S. F. "A numerical model of the structure and evolution of young supernovaremnants," *Mon. Not. Roy. Astron. Soc.*, 1973, **161**, 47
- Jun, B-I. and Norman, M. L. "On the origin of strong magnetic fields in young supernova remnants," *Astrophys. J.*, 1996, **465**, 800
- Levinson A. and Eichler D., "Baryon Purity in Cosmological Gamma-Ray Bursts as a Manifestation of Event Horizons," *Astrophys. J.*, 1993, **418**, 386
- Levinson, A. "Convective instability of a relativistic ejecta decelerated by a surrounding medium: An origin of magnetic fields in GRBs?," *Astrophys. J.*, 2009, **705**, L213

- Lucas, U. Z. and Beloborodov, A. "On the mechanism of Gamma-Ray Burst Afterglows," *Astrophys. J. Lett.*, 2007, **665**, 93
- Lyutikov M. and Blandford, R. D. "Gamma Ray Bursts as Electromagnetic Outflows," *arXiv:astro-ph/0312347*, 2003
- Meszáros, P. and Rees, M. J. "Optical and Long-Wavelength Afterglow from Gamma-Ray Bursts," *Astrophys. J.*, 1997, **476**, 232
- Milosavljevic, M., Nakar E. and Zhang, F. "Vorticity and Magnetic Field Generation from Initial Anisotropy in Ultrarelativistic Gamma-Ray Burst Blastwaves," *arXiv:0708.1588*, 2007
- Nakamura, K. and Shigezuma, T. "Self-similar Solutions for the Interaction of Relativistic Ejecta with an Ambient Medium," *Astrophys. J.*, 2006, **645**, 431
- Panaitescu, A. and P. Kumar, P. "Properties of Relativistic Jets in Gamma-Ray Burst Afterglows," *Astrophys. J.*, 2002, **571**, 779
- Sironi, L. and Goodman, J. "Production of magnetic energy by macroscopic turbulence in GRB afterglow" *Astrophys. J.*, 2007, **671**, 1858
- A. Spitkovsky, "On the Structure of Relativistic Collisionless Shocks in Electron-Ion Plasma" *Astrophys. J.*, 2008, **673**, 39
- Thompson, C. "Deceleration of a relativistic, photon-rich shell: end of preacceleration, damping of magnetohydrodynamic turbulence, and emission mechanism of gamma-ray bursts," *Astrophys. J.*, 2006, **651**, 333
- Wang, X., Loeb, A. and Waxman, E. "Stability of the Forward/Reverse-Shock System Formed by the Impact of a Relativistic Fireball on an Ambient Medium," *Astrophys. J.*, 2002, **568**, 830
- Zhang, W., MacFadyen A. and Wang, P. "Three-Dimensional Relativistic Magnetohydrodynamic Simulations of the Kelvin-Helmholtz Instability: Magnetic Field Amplification by a Turbulent Dynamo," *Astrophys. J. Lett.*, **692**, 40 (2009)